Available online at www.sciencedirect.com

ScienceDirect

MATTER AND RADIATION AT EXTREMES

Matter and Radiation at Extremes 3 (2018) 127−134

www.journals.elsevier.com/matter-and-radiation-at-extremes

Research Article

Self-modulation and anomalous collective scattering of laser produced intense ion beam in plasmas

K. Mima [a,c,*], J. Fuchs [b], T. Taguchi [c], J. Alvarez [d], J.R. Marquès [b], S.N. Chen [b], T. Tajima [e], J.M. Perlado [d]

[a] *The Graduate School for the Creation of New Photonics Industries, 1955-1, Kurematsu, Nishiku, Hamamatsu, Japan*
[b] *LULI − CNRS, Ecole Polytechnique, CEA: Universite Paris-Saclay, UPMC Univ Paris 06: Sorbonne Universites, F-91128, Palaiseau Cedex, France*
[c] *Faculty of Science and Engineering, Setsunan University, Neyagawa, 572-8508, Osaka, Japan*
[d] *Instituto de Fusión Nuclear, ETSI de Industriales, Universidad Politécnica de Madrid, C/ José Gutierrez Abascal, 2, E-28006, Madrid, Spain*
[e] *Department of Physics and Astronomy, University of California at Irvine, Irvine, CA, 92697, USA*

Received 23 July 2017; revised 22 November 2017; accepted 11 December 2017
Available online 15 March 2018

Abstract

The collective interaction between intense ion beams and plasmas is studied by simulations and experiments, where an intense proton beam produced by a short pulse laser is injected into a pre-ionized gas. It is found that, depending on its current density, collective effects can significantly alter the propagated ion beam and the stopping power. The quantitative agreement that is found between theories and experiments constitutes the first validation of the collective interaction theory. The effects in the interaction between intense ion beams and background gas plasmas are of importance for the design of laser fusion reactors as well as for beam physics.

PACS codes: 52.38.Kd; 29.27.Fh; 52.40.Kh; 52.70.Nc

Keywords: Two stream instabilities; Ultra intense short pulse laser; Proton beam; Wake field; Electron plasma wave; Laser plasma interaction

1. Introduction

Proper understanding of collective interaction between ion beams and plasmas is of prime importance for various fields, including the alpha particle interaction with gases in a laser fusion reactor chamber [1], beam propagation in the ion driven fast ignition scheme of inertial confinement fusion [2], collision of plasma bursts from super-nova with inter-stellar gases and collisionless shock wave generation [3−7], and charged particle beam dumping or scattering by gases [8,9]. Theoretical and numerical works have been done to predict collective ion beam-plasma interactions such as the two stream instability and the Weibel instability [3−5].

There are various ion beam instabilities in un-magnetized plasmas. Their growth rates depend upon the beam velocity relative to the ion acoustic velocity, the electron thermal velocity, or the speed of light, the beam velocity spread, the beam density relative to the ambient plasma density, and so on. When the ion beam velocity is higher than the electron thermal velocity, the characteristics of the instabilities are different whether the beam velocity is (1) non-relativistic, or (2) relativistic. In case (1), the instability characteristics are divided into the following two cases: (1)-1 The longitudinal and oblique electron plasma waves are excited by the coupling of a beam mode and an electron plasma wave [10], if the beam velocity spread is smaller than the resonance width of the coupling. It is the so-called "cold beam two stream

* Corresponding author. The Graduate School for the Creation of New Photonics Industries, 1955-1, Kurematsu, Nishiku, Hamamatsu, Japan.
E-mail addresses: k.mima@gpi.ac.jp (K. Mima), julien.fuchs@polytechnique.edu (J. Fuchs).
Peer review under responsibility of Science and Technology Information Center, China Academy of Engineering Physics.

https://doi.org/10.1016/j.mre.2017.12.004

instability" ; (1)-2 On the other hand, when the ion beam velocity spread is larger than the resonance width, namely, the warm beam case, the longitudinal or oblique electron plasma waves and the Weibel mode are excited by the wave particle resonance, namely the "inverse Landau damping". In case (2), when the beam velocity is finite relatively to the speed of light, namely, $\frac{v_b}{c}$ is finite, both electrostatic modes and transverse electromagnetic modes are excited [2−7,11]. The transverse electromagnetic mode is called the "Ion Weibel Instability" [3−7]. Case (2) is relevant to the generation of collisionless shock waves [3−7] where beam density n_b is comparable to plasma electron density n_e.

Although the plasma stopping power of the ion beam from accelerators has been investigated by experiments [12], collective interactions of intense ion beams with hot dense plasmas have not been well investigated experimentally. It is mostly due to the fact that the involved phenomena require extremely large current ion beams such as the alpha particle stream in burning plasmas, or ion streams in the vicinity of super-nova or other particle streams related to extreme events [6].

The generation of intense ion beam by intense short pulse laser (ISPL), however, offers now the unique possibility to explore such collective effects in laboratory. Various mechanisms for ion acceleration by ISPL have been demonstrated experimentally [13−19]. The ion beams emitted as a short pulse from the target source, have naturally a wide energy spectrum and a large number (10^{11}−10^{13}) of particles produced in a single short bunch (ps at the source). The propagation of the laser produced ion beam in vacuum has been investigated in order to characterize the beam emittance, laminarity, and focusability [17,20−22] and to explore its possible applications [19,22]. Its interaction with matter has been proposed as a way to produce hot dense matter [19]. However, no work has addressed the issue of collective interaction of the laser produced ion beams with plasmas.

Here, taking advantage of the unique characteristics of proton beam produced by ISPL, namely its short duration at the source and large number of particles per bunch, we provide the first experimental evidence for the importance of collective interaction effects. It is indeed found that, depending on the beam current density, the characteristics of an ISPL produced high current proton beam could be modified after passing through a plasma jet. The results are found to be in agreement with theoretical predictions based on collective instability theory. In Section 2, we will present the results of our simulations to give the readers a sense of the expected instability growth behavior and its effects on the propagation of the beam. Then, we will show the experimental results (in Sections 3 and 4) as well as an analytical description of the instability that we have observed (in Section 5).

2. Hybrid simulation of ion beam-plasma instabilities

The previous simulations by Kato et al. [3] and Silva et al. [4] investigated the two stream instability for counter-streaming plasmas. In their cases, the growth rate of the electro-magnetic transverse instability like ion Weibel instability is comparable to that of the electrostatic instabilities. In particular, in the nonlinear regime, the magnetic field fluctuations are dominant. On the other hand, in the present laboratory experiments, the proton beam is weakly relativistic, namely $\frac{v_b}{c} \sim 0.1$ and the beam density is much less than the ambient plasma density. In this case, the electrostatic or weak electromagnetic instabilities are dominant and the nonlinear behavior of the proton beam is different from the previous cases [3,4]. In order to investigate the linear and nonlinear developments of the beam instabilities, we carried out large scale hybrid simulations [23] and compared the results with the experimental ones.

In our instability analysis, the proton beam density varies from 10^{-1} to 10^{-5} of the ambient plasma electron density and the beam energy is 4−10 MeV for comparison with the experiments discussed in Section 3. For the same reason, we fix the ambient plasma electron density to be 4×10^{19} cm^{-3}. When the proton beam propagates from the laser irradiation target to the gas jet, the proton beam pulse spreads in space and time. In the beam spreading process, the local velocity spread of the beam is reduced to be $\frac{\Delta v_b}{v_b} \sim \frac{\Delta d}{d} \sim \frac{\Delta t}{t}$, where Δd is the acceleration distance ~10μm, d is the distance between the proton source and the gas plasma ~4 mm, Δt is the acceleration time ~0.1 ps [24,25], and t is the time-of-flight from the source to the gas plasma ~50 ps. Then, the beam temperature in the interaction region is estimated to be $M\frac{(\Delta v_b)^2}{2} \sim 10^{-5} M\frac{v_b^2}{2} < 100$ eV. This is the reason that we assume the beam temperature is 100 eV in the simulation and it is consistent with the experimental findings [26].

The linear dispersion relation for the ion beam instability reported in the works [3,27,28] is solved numerically to observe the longitudinal and oblique mode growth rates. The growth rates for the ion beam instability of various ion beam densities are shown in Fig. 1, where the ion beam velocity spread is assumed to be 0.35%. When the beam density is higher than 0.1% of the plasma electron density, the growth rate is proportional to the cubic root of the beam density as shown by a broken line in Fig. 1(a), which represents the cold beam instability. On the other hand, when the beam density is much smaller than 0.1% of the ambient plasma electron density, the instability is due to the inverse Landau damping and the growth rate is proportional to the beam density. We note here that when the Doppler shift frequency due to the beam velocity spread $k\Delta v_b$ is larger than the cold beam growth rate which is actually the resonance width of the beam mode coupling, the instability becomes kinetic, namely, the instability is due to the inverse Landau damping.

As shown in Fig. 1(a), the maximum growth rate is higher than $10^{-4}\omega_{pe}$ when $\frac{n_b}{n_e} > 10^{-5}$ and is finite. For the plasma density of 4×10^{19}cm^{-3}, the growth length $\frac{v_b}{\gamma_{max}} \sim 0.7$ mm. Therefore, the electron plasma waves could grow significantly, if the plasma length is longer than a few millimeters, which is the case in our experiment and will be discussed later. Fig. 1(b) shows that the transverse wave number of the

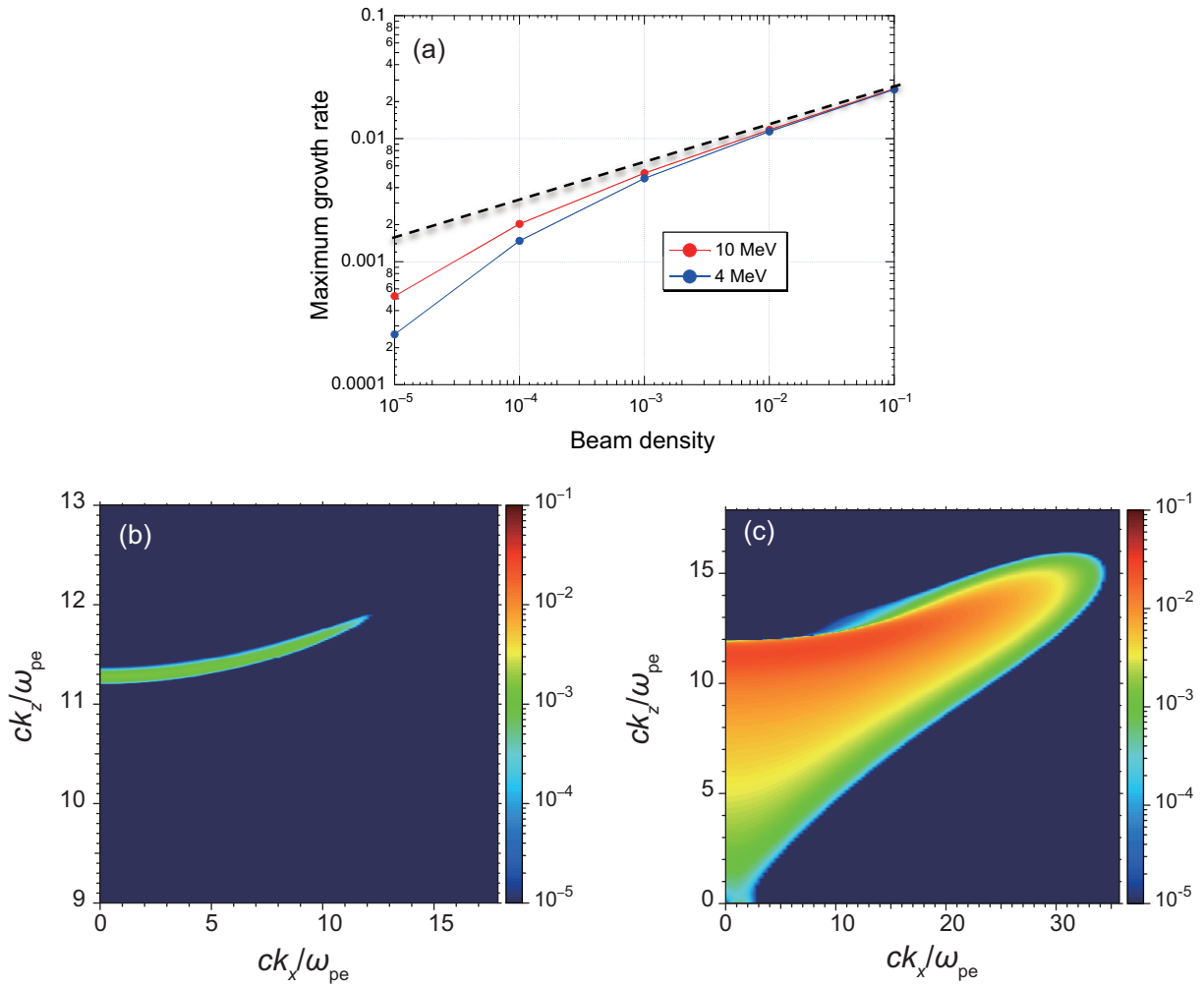

Fig. 1. (a) Beam density (normalized by the plasma electron density) dependence of the maximum growth rate (normalized by the plasma frequency) for the ion beam, where the broken line shows the cubic root of the beam density. Colors in the wave number space indicate the growth rate normalized by ω_{pe} for (b) $\frac{n_b}{n_e} = 10^{-4}$ and (c) $\frac{n_b}{n_e} = 10^{-1}$.

unstable modes is comparable to the longitudinal wave number. Namely, the transverse electric field is comparable to the longitudinal fields. So the ion beam not only loses energy but also scatters. When the beam density is higher, the unstable region is wider (as shown in Fig. 1(c)) and the transverse wave number of unstable modes is comparable or larger than the longitudinal wave number. The frequency of unstable modes near the k_x-axis is much lower than the electron plasma frequency and those modes are Weibel-like.

The two-dimensional electro-magnetic hybrid simulation code developed by T. Taguchi et al. [23] has been applied to investigate the nonlinear evolution of the ion beam instability.

The hybrid code is better to simulate long timescale and large spatial scale phenomena than PIC, because the mesh size Δx can be larger than the Debye length and the time step $\Delta\tau < \frac{\Delta x}{c}$ can be larger. Therefore, we applied the hybrid code where the electron motion is described by the fluid equations.

Here, the ambient electrons are described by the fluid equations and the background ions and beam ions are described by particles with full Maxwell equations. In Fig. 2, the ion beam is injected from the left boundary at $z = 20\frac{c}{\omega_{pe}}$ continuously into the uniform plasma of which the electron density is $n_e = 4 \times 10^{19}\text{cm}^{-3}$, and particles and electromagnetic fields are absorbed in the right boundary at $z = 250\frac{c}{\omega_{pe}}$. Fig. 2(a)–(d) show respectively the spatial distributions of the longitudinal and transverse electric fields, the ion beam density distributions and magnetic field at the end of the simulation for the parameters related to the experiments, except for the beam density which was taken as $\frac{n_b}{n_e} = 0.01$. Such higher beam density was selected in order to investigate the full nonlinear evolution of the instabilities within the possible simulation box size. Fig. 2(a) and (b) show that the longitudinal and transverse electric fields grow spatially from the left boundary, as the beam density fluctuations and the magnetic fields shown in Fig. 2(c) and (d) respectively.

The ion beam breaks up into small fragments to generate electron plasma waves in the saturated state. The maximum longitudinal electric field amplitude reaches 10^9 V/m for

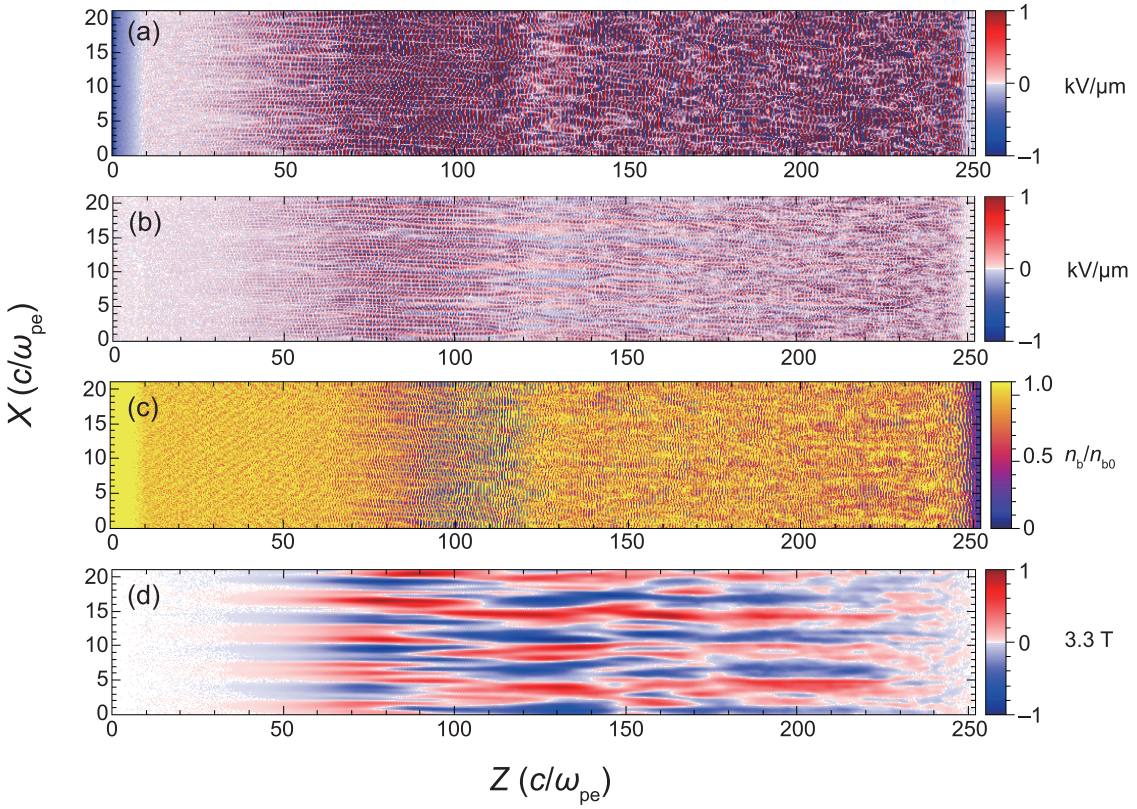

Fig. 2. Hybrid simulation of the two stream instability of the ion beam. The right-hand writings are the units of color bars. The plasma electron density is $4 \times 10^{19}\mathrm{cm}^{-3}$ and the proton beam density is 1% of the plasma density. (a) and (b) are the longitudinal and transverse electric field distribution respectively, (c) and (d) are the proton beam density distribution and B_z distribution respectively at 340 ps after starting the proton beam injection from the left.

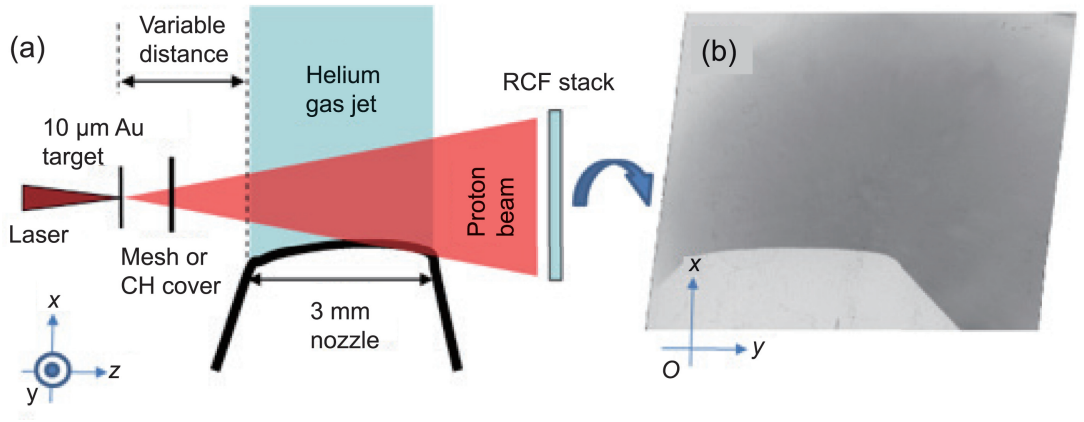

Fig. 3. (a) Schematic of experiment. The laser pulse, focused on an Au thin foil, generates a proton beam that probes a He gas jet pressurized at 100 bars. The distance between the proton source and the jet is varied. Protons are detected on multiple layers of RCFs. (b) Example of a proton radiograph (at 4 MeV) in the absence of gas in the nozzle. The shadow of the nozzle is clearly visible.

0.1 mm propagation length (see Fig. 2(a)). Note also that the transverse electric field is comparable to the longitudinal electric field as shown in Fig. 2(b).

The simulation indicates that the electric fields build-up distance is about 5 times the e-folding distance, which is 0.05 mm $\left(\sim 5\frac{v_b}{\gamma_{max}}\right)$ according to Fig. 2(c), in the case of $\frac{n_b}{n_e} = 0.01$. Fig. 2(c) shows that the proton beam is strongly modulated by the electric field and there is a density compression at $100\frac{c}{\omega_p}$ from the injection point. Fig. 2(d) shows that modest magnetic fields are generated due to the transverse ion current modulation.

For $\frac{n_b}{n_e} = 10^{-5}$ as in the experiments described in the next section, the fluctuating electric fields will build up at the distance of 3.5 mm, where $\frac{v_b}{\gamma_{max}} \sim 0.7$ mm according to Fig. 1(a). Accordingly, the ion beam may break up into tiny clusters induced by the instabilities which will saturate. Therefore, the

electric field growth is expected to be saturated after the beam propagates for longer than 3.5 mm.

3. Experimental set-up

The beam-plasma interaction experiment was performed using the 100 TW ISPL at the Laboratoire pour l'Utilisation des Lasers Intenses (LULI). The concept of the experiment is shown schematically in Fig. 3(a). The high-current ion beam is produced by irradiating a metallic thin foil (10 μm thick Au) with a short-pulse, ultra-high intensity laser (~20–30 J of 1 μm light with 350 fs duration, focused to ~10^{19} W/cm^2) [16–18]. Laser-generated fast electrons set a ~TV/m electrostatic sheath field [16,22] on the target rear surface; the field ionizes the surface atoms and accelerates the resulting ions, which are mostly protons originating from the surface contaminant layers (water vapor and hydrocarbons) [15,19]. The protons are detected using multiple layers of radiochromic film (RCF) [15,29]. The spatial distribution of protons in a given RCF layer gives the angular emission pattern at a specific interval of proton energy. By carefully preparing the rear surface of the target foil [16], and by controlling the laser focal intensity distribution using a deformable mirror [30], the proton beam can be generated in a laminar fashion [17,20,21] with a smooth angular distribution [16] and an energy spectrum that ranges from 4 to 10 MeV. Approximately 10^{11} protons are produced in a single laser-shot for energies above 4 MeV. Due to the energy spread of the beam, the proton current varies from ~1 kA at 1 mm from the plasma source to ~100 A at 1 cm. Due to the beam divergence of ~10° half-angle, the beam current density also decreases rapidly with the distance from the target (1 MA/cm^2 at 1 mm and 1 kA/cm^2 at 1 cm). The proton beam is then propagated through a supersonic jet of He coming from a conical nozzle with 100 bars backing pressure which is open for ~10 ms before the laser shot. The equivalent electron density of the fully ionized jet at this pressure is ~4×10^{19} cm^{-3}. We can assume that the gas jet is ionized first by the front of laser accelerated electrons injected into the plasma [31]. Indeed, the strong high energy electron pulse may induce strong electric fields which lead to gas discharge following which further ionization of the gas will take place [32].

4. Experimental results on ion beam interaction with a gas target

As shown in Fig. 3(b), the protons in the plasma beam did not present any noticeable structures without triggering the jet, and the proton beam profile was smooth. However, when we injected gas in the nozzle, we observed, depending on the proton beam current at the gas jet location, strong modulations in the proton beam after passing through the gas, as shown in Fig. 4.

Lighter zones on the films correspond to areas where protons are deflected and defocused by the interaction with the gas jet. Conversely, darker zones correspond to local focusing of the beam. It is determined that the modulations are due to the interaction between the proton beam and the gas jet, and not to a perturbation of the acceleration on the solid target surface induced by the gas flowing from the jet. Indeed, when positioning a fine mesh in between the solid target and the jet (see Fig. 3(a)), we observed that the image of the mesh was distorted, indicating that distortions had taken place in the gas jet (see Fig. 4(b)). If the proton beam was simply modulated at the source, i.e. before the mesh, and was not perturbed by the jet, density modulations would appear but the mesh would impose a regular pattern on the beam. Here, the pattern imprinted by the mesh is seen to be distorted, indicating that the distortions took place after the mesh. Consistently, we see that the mesh distortions followed the proton beam density modulations very closely. Moreover, we placed a 4 μm CH film in between the target and the gas jet to prevent any possible contamination of the proton source foil and still observed the modulations.

As shown in Fig. 5, modulations in the lower energy proton beam are more pronounced than those in the higher energy proton beam. Namely, the lower energy part of the proton beam has a higher density and also crosses the jet at a later time (at 4 mm from the source, the time-of-flight difference between 4 MeV and 10 MeV protons is ~53 ps). Also, as observed in Fig. 4, the modulations are stronger when the plasma beam source is closer from the jet, in which case the spread of the beam due to the angular divergence is still small and the beam density is higher. The modulations are not only reduced with the beam density but also with the density of the

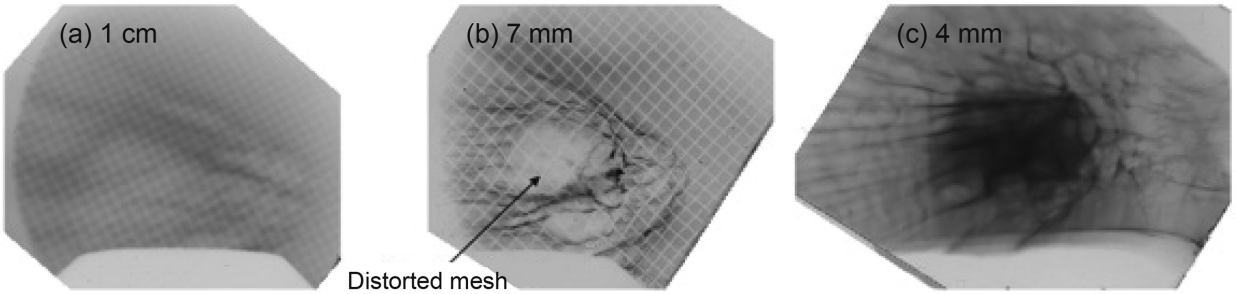

Fig. 4. Proton beam pattern (at 4 MeV) after passing through the gas jet with the distance from the proton source to the middle of the jet being (a) 1 cm, (b) 7 mm and (c) 4 mm.

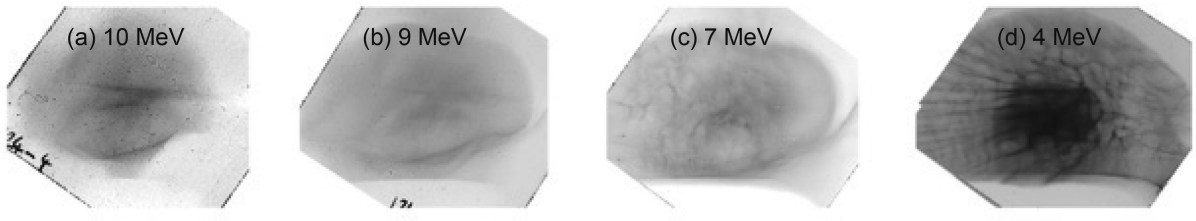

Fig. 5. Proton beam patterns after passing through the gas jet and observed at different proton energies as indicated with the distance from the proton source to the middle of the jet being kept at 4 mm. All films correspond to various proton energies produced and propagated through the gas in a single shot.

jet. When reducing the backing pressure to 35 bars, the perturbations on the proton beam are virtually suppressed, even when positioning the proton source at 4 mm from the gas.

5. Analysis of the experimental results by beam plasma instabilities

Let us now compare the collective interactions of the proton beam with the gas jet in the simulations and experiments. According to the experimentally measured proton beam distribution, the proton beam density at L (cm), the center of the gas jet is obtained as

$$n_{\mathrm{b}}(L,t)=\frac{6.54\times10^{13}}{\pi L^3}\,\frac{E}{2.6\ [\mathrm{MeV}]}\exp\left(\frac{4.0-E}{2.6\ [\mathrm{MeV}]}\right)\left[\mathrm{cm}^3\right] \quad (1)$$

Note that Eq. (1) is derived by using the relation:

$$\int_{L_0}^{\infty}2\pi L^2(1-\cos\theta)n_{\mathrm{b}}(L,t)=\int_{4.0\ [\mathrm{MeV}]}^{\infty}\mathrm{d}E\frac{\mathrm{d}N}{\mathrm{d}E}=10^{11}$$

and

$$\mathrm{d}E=\frac{M_{\mathrm{b}}L}{t^2}\mathrm{d}L,$$

where 10^{11} is the number of the detected total protons with energy higher than 4.0 MeV.

Here, we note that: $\mathrm{d}N/\mathrm{d}E=(10^{11}/2.6)\ \exp[(4.0\ \mathrm{MeV}-E)/2.6\ \mathrm{MeV}]$, which is the divergence half angle, $E=M_{\mathrm{b}}(L/t)^2/2$ is the energy of a proton arriving at L, and we assume a proton of 4.0 MeV arriving at L_0 at the time t with a proton mass M_{b}. L is the distance from the target rear surface to the center of the gas jet.

We will consider here the electro-static and electromagnetic beam instabilities that can take place when an intense ion beam interacts with gas plasmas. When $v_{\mathrm{b}}/v_{\mathrm{e}}$ (electron thermal velocity) >1, both ion and electron modes are destabilized and the ion–ion two stream instability [9] and the Weibel instability [3,11,29] can take place. As for the Weibel instability, the maximum growth rate is $\omega_{\mathrm{b}}v_{\mathrm{b}}/c$ [11] for ion beam plasma frequency $\omega_{\mathrm{b}}=(n_{\mathrm{b}}Z_{\mathrm{b}}^2e^2/\varepsilon_0M_{\mathrm{b}})^{1/2}$, plasma ion mass M_{i} and ion charge Z_{i} which is about $2\times10^{10}\ \mathrm{s}^{-1}$. The corresponding e-folding time is 50 ps, which is comparable to the proton beam pulse width (53 ps). Therefore, the Weibel instability is not taken into account hereafter.

For a cold ion beam and low electron temperature plasmas, the dispersion relation for the electro-static wave [10] is approximately given by:

$$1-\frac{\omega_{pe}^2}{(\omega+i\nu)^2}-\frac{\omega_{pi}^2}{\omega^2}-\frac{\omega_{\mathrm{b}}^2}{\left(\omega-k_{\|}v_b\right)^2}=0, \quad (2)$$

where $\omega_{\mathrm{pe}}=(n_{\mathrm{e}}e^2/\varepsilon_0m)^{1/2}$ and $\omega_{\mathrm{pi}}=(n_{\mathrm{i}}Z_{\mathrm{i}}^2e^2/\varepsilon_0M_{\mathrm{i}})^{1/2}$ are the electron and ion plasma frequencies of the ambient plasma, $k_{||}$ is the wave vector parallel to the beam and ν is the electron-ion collision frequency. Here, n_{e} and n_{i} are the densities of electrons and ions, respectively. When $n_{\mathrm{b}}/n_{\mathrm{i}}\ll1$, the frequency of the unstable mode is close to $\omega=k_{||}v_{\mathrm{b}}$. In the case of low electron temperature, namely, $kv_{\mathrm{e}}<k_{||}v_{\mathrm{b}}\sim\omega_{\mathrm{pe}}$, the cold electron approximation (Eq. (2)) is applicable. Then, the dispersion relation of the unstable electron plasma wave, Eq. (2), is reduced to

$$\left(\omega^2-\omega_{\mathrm{pe}}^2\right)\left(\omega-k_{\|}v_{\mathrm{b}}\right)^2=\omega_{\mathrm{b}}^2\omega^2, \quad (3)$$

if the collision frequency is small enough, namely, $\nu\ll(\omega_{\mathrm{b}}^2\omega_{\mathrm{pe}})^{1/3}$. When $k_{||}v_{\mathrm{b}}<\omega_{\mathrm{pe}}$, the dispersion relation Eq. (3) yields, $\omega=k_{||}v_{\mathrm{b}}+\mathrm{i}\Gamma$, where $\Gamma=\omega_{\mathrm{b}}k_{\mathrm{b}||}v_{\mathrm{b}}/[\omega_{\mathrm{pe}}^2-(k_{||}v_{\mathrm{b}})^2]^{1/2}$. This indicates that the unstable electron wave propagates with the ion beam velocity and the growth rate Γ increases when $k_{||}v_{\mathrm{b}}$ approaches ω_{pe}. The growth rate becomes maximum when $k_{||}v_{\mathrm{b}}=\omega_{\mathrm{pe}}$, then Eq. (3) yields

$$\omega=k_{\|}v_{\mathrm{b}}+\exp\left(\frac{2\pi\mathrm{i}}{3}\right)\omega_{\mathrm{pe}}\left(\frac{mn_{\mathrm{b}}}{2M_{\mathrm{b}}n_{\mathrm{e}}}\right)^{1/3}.$$

Namely,

$$\frac{\Gamma}{\omega_{\mathrm{pe}}}=\frac{3^{1/2}}{2}\left(\frac{mn_b}{2M_{\mathrm{b}}n_{\mathrm{e}}}\right)^{1/3}\sim6\times10^{-2}\left(\frac{n_{\mathrm{b}}}{n_{\mathrm{e}}}\right)^{1/3}. \quad (4)$$

In the experiment, the plasma electron temperature may be ~100 eV. Thus, $\nu/\omega_{\mathrm{pe}}\sim10^{-3}$ and $\nu<\Gamma$.

Using the proton beam density at the center of the jet given by Eq. (1) and the growth rate given by Eq. (4), we evaluated the growth rate and the amplification factor of the instability. The results are summarized in Table 1. The parameters used in Table 1 correspond to the distances employed in the three cases of Fig. 4, namely (a), (b), and (c) and to the beam energies of Fig. 5. As it is

apparent from the growth rate and the amplification factors, we conclude that the proton beam driven electro-static instability is effective for a 4.0 MeV beam interacting with the gas jet at the distance of 4 mm, whereas it becomes marginal when (1) the beam energy increases to 10 MeV (still for the distance of 4 mm), or (2) the distance increases to 10 mm, while the energy is kept at 4 MeV. The other cases, i.e. higher beam energies or larger distances, display even lower growth rates, hence reveal low levels of beam instabilities. These theoretical estimates are well consistent with the experimental results of Figs. 4 and 5.

In order to quantitatively compare our estimates to the experimental data, we now evaluate the possible deflection angle impaired on the proton beam induced by a well-developed instability. Let us assume that the ion beam density is spatially modulated as $\frac{\delta n_b}{n_b} = A\cos(k_\perp r + k_\parallel z - k_\parallel v_b t)$ by the instability. Then the modulations excite wake fields in the gas jet plasma. The wake fields will subsequently scatter the proton beam. The wake fields are evaluated as,

$$eE = K/\|k\| \left[\frac{n_b \omega_{pe}^2}{\varepsilon(k_\parallel v_b) k_\parallel v_b n_e} m v_b \frac{A}{2i} \exp\left(i\left(k_\perp r + k_\parallel z - k_\parallel v_b t\right)\right) + \text{c.c.} \right],$$

where $\varepsilon(\omega) = 1 - \frac{\omega_{pe}^2}{\omega(\omega + i\nu)}$ is the longitudinal dielectric constant for the cold electron plasma. Since $k_\parallel v_b = \omega_{pe}$, and $\nu \ll \omega_{pe}$, we get

$$eE = K/\|k\| \frac{\omega_{pe}^2}{\nu} \frac{n_b}{n_e} m v_b A \cos\left(k_\perp r + k_\parallel z - k_\parallel v_b t\right). \quad (5)$$

When A~0.5, and $n_e = 4 \times 10^{19}\text{cm}^{-3}$, $\frac{n_b}{n_e} = 2 \times 10^{-6}$ (i.e. corresponding to the 7 mm distance), $v_b = 2.8 \times 10^9$ cm/s, and ν/ω_{pe}~10^{-3}, the electric field of the wake-field reaches 6.0×10^7 V/m. When the distance decreases to 4 mm (resp. increases to 1 cm), the electric field is 3.0×10^8 V/m (resp. 1.9×10^7 V/m).

Fig. 6 shows the experimental modulation of the ion beam dose as recorded on the RCF for the 4 mm and 7 mm cases (i.e. the curve correspond to line outs of the images shown in Fig. 4(b) and (c)). Fig. 6 indicates that the scattering angle of ions is about 0.02 rad for the 4 mm case. So, the transverse modulation velocity is estimated to be about 10^8 cm/s for 4 MeV protons. It is obvious that the shorter the distance, the deeper the modulations, hence the stronger the E-field that leads to the modulations. Thus, the trend is already consistent with the theoretical estimate of Eq. (5). Qualitatively, the beam modulation in the gas jet plasma is as expected by the simulation (see Fig. 2). We can go one step further and retrieve quantitative estimates of the electric fields inducing the observed proton deflections from the lineouts and knowing that the distance between the gas jet and the RCF is 63.5 mm. This is made using a particle tracing program [33]. In these simulations, we observe that the depth of the dose modulation depends essentially on the strength of the E-field in the plasma. We can thus infer the following estimate of the E-fields: $(3-5)\times10^8$ V/m for 4 mm, $(4-7)\times10^8$ V/m for 7 mm, $(1-4)\times10^8$ V/m for 1 cm, in very good agreement with the theoretical estimates and simulation results given above.

Table 1
Growth rate (upper) and amplification e-foldings (lower) of the proton beam driven electrostatic instability, for the proton source target/gas jet distances and proton energies considered here and that correspond to the experimental data of Figs. 4 and 5.

Distance	Energy		
	4 (MeV)	7 (MeV)	10 (MeV)
4 (mm)	5.4×10^{11} (s^{-1})	4.8×10^{11} (s^{-1})	3.6×10^{11} (s^{-1})
	55 (see Fig. 2(c))	30 (see Fig. 3(c))	16 (see Fig. 3(a))
7 (mm)	3.1×10^{11} (s^{-1})	2.7×10^{11} (s^{-1})	2.0×10^{11} (s^{-1})
	26 (see Fig. 2(b))	17	9.5
10 (mm)	2.2×10^{11} (s^{-1})	1.9×10^{11} (s^{-1})	1.4×10^{11} (s^{-1})
	14 (see Fig. 2(a))	12	6.8

6. Discussions

The presented analysis of the importance of collective effects in the interaction between an ion beam and a plasma has implications on laser fusion reactor design, since a similar situation could happen for the burning plasma interaction with chamber gas contained in a laser fusion reactor. For example, the 3.5 MeV alpha particles produced by D-T reactions escape from the burning plasma, of about 100 μm radius, with velocity $v_b = 1.5 \times 10^9$ cm/s and their density which drops as they propagate across the chamber is about $n_b = 10^{13}$ cm^{-3} at 1 m from the center. If the chamber gas pressure (higher than 10 mTorr [1]) is ionized by strong X-ray radiation, the alpha particles will deposit significant energy into the gas. In the case that all or part of the energy of the ions is transferred to the surrounding gas, the energy deposition on the first wall would be then more bearable since the time scale of the energy deposition would be long, due to the convective and radiative heat transfer between gas and wall [34]. However, the ion-gas energy transfer could also cause unwanted effects in the propagation of the laser pulses or of the targets to the target chamber. For example, deviations from the selected trajectory of the injected target or excessive heating of the cryogenically cooled D-T fuel may arise from the hot and surely turbulent background gas if it has not been cooled down before the next fusion shot.

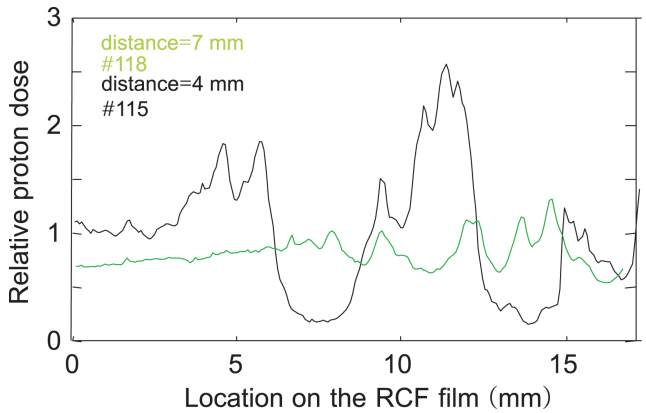

Fig. 6. Beam intensity fluctuations as recorded on the RCF. The black solid curve is for 4 mm and the green curve is for 7 mm distance from the proton source target to the gas jet.

Conflict of interest

The authors declare that there is no conflicts of interest.

Acknowledgments

K. Mima thanks Universidad Politécnica de Madrid for supporting this research through the guest professor program. We thank V. I. Sotnikov for fruitful discussions. J. Alvarez thanks the Spanish MINECO for support via the ACI-PROMOCIONA program 2011 (AIC-A-2011-0718). We acknowledge the support of the LULI technical teams and support from Grant No. E1127 from Région Ile-de-France. S.N.C is supported by the National Science Foundation under Grant No. OISE-1064468. This work was partly done within the LABEX Plas@Par project and supported by Grant No. 11-IDEX-0004-02 and ANR-17-CE30-0026-Pinnacle from Agence Nationale de la Recherche. It has received funding from the European Union's Horizon 2020 Research and Innovation programme under LASERLAB-EUROPE grant agreement No. 654148 Laserlab-Europe. This work has been carried out within the framework of the EUROfusion Consortium and has received funding, through the ToIFE, from the European Union's Horizon 2020 research and innovation programme under Grant Agreement No. 633053. The views and opinions expressed herein do not necessarily reflect those of the European Commission. This work was also supported in part by JSPS KAKENHI Grant No. 15H03758.

References

[1] F. Najmabadi, A.R. Raffray, ARIES-IFE Team, S.I. Abdel-Khalik, L. Bromberg, et al., Operational windows for dry-wall and wetted-wall IFE chambers, Fusion Sci. Technol. 46 (2004) 401–416.
[2] M. Roth, T.E. Cowan, M.H. Key, S.P. Hatchett, C. Brownet, et al., Fast ignition by intense laser-accelerated proton beams, Phys. Rev. Lett. 86 (2001) 436–439.
[3] T.N. Kato, H. Takabe, Electrostatic and electromagnetic instabilities associated with electrostatic shock: two-dimensional particle-in-cell simulation, Phys. Plasmas 17 (2010) 03211-1-10.
[4] L.O. Silva, M. Marti, J. Davies, R.A. Fonseca, C. Ren, et al., Proton shock acceleration in laser-plasma interaction, Phys. Rev. Lett. 92 (2004) 015002-1-4.
[5] G. Sorasio, M. Marti, R. Fonseca, L.O. Silva, Very high mach-number electrostatic shocks in collision-less plasmas, Phys. Rev. Lett. 96 (2006) 045005-1-4.
[6] E. Baldwin, Shock Wave Blasts Through Galaxy, 2009. Astronomy Now, Posted: 23 April.
[7] T. Amano, M. Hoshino, Electron shock surfing acceleration in multi-dimensions: two-dimensional particle-in-cell simulation of collision-less perpendicular shock, APJ 690 (2009) 244–251.
[8] H.-C. Wu, T. Tajima, D. Habs, A.W. Chao, J. Meyer-ter-Vehn, Collective deceleration: toward a compact beam dump, Phys. Rev. Spec. Top. Accel. Beams 13 (2010) 101303-1-8.
[9] E.A. Starstev, R.C. Davidson, M. Dorf, Two-stream stability properties of the return-current layer for intense ion beam propagation through background plasma, Phys. Plasmas 16 (2009) 092101-1-8.
[10] F.F. Chen, Introduction to Plasma Physics and Controlled Fusion, second ed., Plenum Press, New York, 1984. Chapt. 6.
[11] A. Bred, M.C. Firpo, C. Deutsch, Characterization of the initial filamentation of a relativistic electron beam passing through a plasma, Phys. Rev. Lett. 94 (2005) 115002-1-4.
[12] A. Frank, A. Blažević, P.L. Grande, K. Harres, T. Heßling, et al., Energy loss of argon in a laser-generated carbon plasma, Phys. Rev. E 81 (2010) 026401-1-6.
[13] S.P. Hatchett, C.G. Brown, T.E. Cowan, E.A. Henry, J.S. Johnson, Electron, proton, and ion beam from the relativistic interaction of petawatt laser pulses with solid targets, Phys. Plasmas 7 (2000) 2076–2082.
[14] E.L. Clark, K. Krushelnick, J.R. Davies, M. Zepf, M. Tatarakis, et al., Measurements of energetic proton transport through magnetized plasma from intense laser interactions with solids, Phys. Rev. Lett. 84 (2000) 670–673.
[15] R.A. Snavely, M.H. Key, S.P. Hatchett, T.E. Cowan, M. Roth, et al., Intense high-energy proton beams from petawatt-laser irradiation of solids, Phys. Rev. Lett. 85 (2000) 2945–2948.
[16] J. Fuchs, T.E. Cowan, P. Audebert, H. Ruhl, L. Gremillet, et al., Spatial uniformity of laser-accelerated ultra high current MeV electron propagation in metals and insulators, Phys. Rev. Lett. 91 (2003) 255002-1-4.
[17] T.E. Cowan, J. Fuchs, H. Ruhl, A. Kemp, P. Audebert, et al., Ultralow emittance, multi-MeV proton beams from a laser virtual cathode plasma accelerator, Phys. Rev. Lett. 92 (2004), 204801-1-4.
[18] P. Mora, Thin-foil expansion into a vacuum, Phys. Rev. E 72 (2005) 056401-1-5.
[19] M. Borghesi, J. Fuchs, S.V. Bulanov, A.J. Mackinnon, P.K. Patel, et al., Fast ion generation by high-intensity laser irradiation of solid targets and applications, Fus. Sci. Technol. 49 (2006) 412–439.
[20] M. Roth, A. Blazevic, M. Geissel, T. Schlegel, T.E. Cowan, et al., Energetic ions generated by laser pulses: a detailed study on target properties, Phys Rev ST-AB 5 (2002) 061301-1-8.
[21] S. Ter-Avetisyan, M. Borgheshi, M. Schnurer, P.V. Nickles, W. Sandner, et al., Characterization and control of ion sources from ultra-short high-intensity laser-foil interaction, Plasma Phys. Control. Fusion 51 (2009) 124046-1-8.
[22] M. Borghesi, A.J. Mackinnon, D.H. Campbell, D.G. Hicks, S. Ker, et al., Multi-MeV proton source investigations in ultraintense laser-foil interactions, Phys. Rev. Lett. 92 (2004) 055003-1-4.
[23] T. Taguchi, T.M. Antonsen Jr., K. Mima, Study of hot electron beam transport in high density plasma using 3D hybrid-Darwin code, Comput. Phys. Commun. 164 (2004) 269–278.
[24] A. Flacco, F. Sylla, M. Veltcheva, M. Carrié, et al., Dependence on pulse duration and foil thickness in high-contrast-laser proton acceleration, Phys. Rev. E 81 (2010) 036405.
[25] S. Fourmaux, S. Buffechoux, B. Albertazzi, D. Capelli, A. Levy, et al., Investigation of laser-driven proton acceleration using ultra-short, ultra-intense laser pulses, Phys. Plasmas 20 (2013) 013110.
[26] A. Kemp, J. Fuchs, Y. Sentoku, V. Sotnikov, M. Bakeman, et al., Emittance growth mechanisms for laser-accelerated proton beams, Phys. Rev. E 75 (2007) 056401.
[27] S. Ichimaru, Basic Principles of Plasma Physics, 1973. Reading, MA.
[28] B. Hao, W.J. Ding, Z.M. Sheng, C. Ren, J. Zhang, Plasma thermal effect on the relativistic current-filamentation and two-stream instabilities in a hot-beam warm-plasma system, Phys. Rev. E 80 (2009) 066402-1-5. K.M. Watson, S.A. Bludman, M.N. Rosenbluth, Statistical mechanics of relativistic streams I, Phys. Fluids 3, 741–747(1960).
[29] N.V. Klassen, L. van der Zwan, J. Cygler, GafChromic MD-55: investigated as a precision dosimeter, Med. Phys. 24 (1997) 1924–1934.
[30] B. Wattellier, J. Fuchs, J.P. Zou, K. Abdeli, H. Pépin, et al., Repetition rate increase and diffraction-limited focal spots for a nonthermal-equilibrium 100-TW Nd:glass laser chain by use of adaptive optics, Opt. Lett. 29 (2004) 2494–2496.
[31] R.B. Miller, On electron beam propagation in neutral gases, in: An Introduction to the Physics of Intense Charged Particle Beams, 1982. Plenum, New York.
[32] Y.A. Omelchenko, V.I. Sotnikov, V.D. Shapiro, V.I. Shevchenko, Strong Langmuir turbulence and beam plasma discharge in the ionospheric plasma, Planet. Space Sci. 40 (1992) 535–540.
[33] L. Lancia, M. Grech, S. Weber, J.-R. Marquès, L. Romagnani, et al., Anomalous self-generated electrostatic fields in nanosecond laser-plasma interaction, Phys. Plasmas 18 (2011) 030705.
[34] J. Alvarez, D. Garoz, R.G. Arrabal, A. Ribera, M. Perlado, The role of spatial and temporal radiation deposition in inertial fusion chambers: the case of HiPER, Nucl. Fusion 51 (2011) 053019-1-5.